Femtosecond Transient Absorption, Nanosecond Time-Resolved Resonance Raman, and Density Functional Theory Study of Fenofibric Acid in Acetonitrile and Isopropyl Alcohol Solvents

ARTICLE *in* THE JOURNAL OF PHYSICAL CHEMISTRY A · NOVEMBER 2011

Impact Factor: 2.69 · DOI: 10.1021/jp207582w · Source: PubMed

THE JOURNAL OF PHYSICAL CHEMISTRY A

ARTICLE

pubs.acs.org/JPCA

Femtosecond Transient Absorption, Nanosecond Time-Resolved Resonance Raman, and Density Functional Theory Study of Fenofibric Acid in Acetonitrile and Isopropyl Alcohol Solvents

Ming-De Li,[†] Wen Li,[†] Jiani Ma,[†] Tao Su,[†] Mingyue Liu,[†] Yong Du,[‡] and David Lee Phillips*[,†]

[†]Department of Chemistry, The University of Hong Kong, Pokfulam Road, Hong Kong S.A.R., P. R. China

[‡]Centre for THz Research, China Jiliang University, Hangzhou 310018, P. R. China

Supporting Information

ABSTRACT: Hydrogen abstraction reaction of fenofibric acid (FA) in acetonitrile and isopropyl alcohol solvents was studied by femtosecond transient absorption (fs-TA) and nanosecond time-resolved resonance Raman (ns-TR^3) spectroscopy experiments. The singlet excite state (^{1}FA) (nπ^*) with a maximum transient absorption at 352 nm observed in the fs-TA experiments undergoes efficient intersystem crossing (ISC) to convert into a nπ^* triplet state FA (^{3}FA) that exhibits two transient absorption bands at 345 and 542 nm. The nπ^* ^{3}FA species does not decay obviously within 3000 ps. In the ns-TR^3 experiments, the nπ^* ^{3}FA is also observed and completely decays by 120 ns. Compared with the triplet states of benzophenone (BP) and ketoprofen (KP), the nπ^* ^{3}FA species seems to have a much higher hydrogen abstraction reactivity so that ^{3}FA decays fast and generates a FA ketyl radical like species. In isopropyl alcohol solvent, the nπ^* ^{3}FA exhibits similar reactivity and promptly abstracts a hydrogen from the strong hydrogen donor isopropyl alcohol solvent to generate a ketyl radical intermediate. With the decay of the FA ketyl radical, no light absorption transient (LAT) intermediate is observed in isopropyl alcohol solvent although such a LAT species was observed after similar experiments for BP and KP. Comparison of the ns-TR^3 spectra for the species of interest with results from density functional theory calculations were used to elucidate the identity, structure, properties, and major spectral features of the intermediates observed in the ns-TR^3 spectra. This comparison provides insight into the structure and hydrogen abstraction reactivity of the triplet states of BP derivatives.

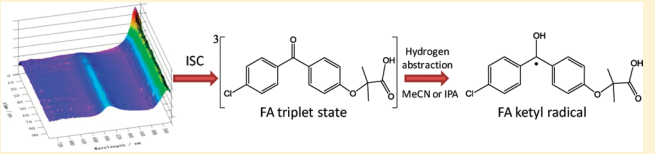

INTRODUCTION

The photochemistry of a number of pharmaceutical products have received much attention due to reports about adverse photosensitization reactions produced by photosensitive chromophores in certain drugs.[1] In particular, drugs containing benzophenone (BP) derivatives often have a high quantum efficiency of the intersystem crossing (ISC) that transforms from the singlet excited state to a reactive triplet state that may undergo damaging reactions with biological molecules.[2] For BP derivatives, the electronic configuration of the T_1 state will determine the T_1 state's reactivity toward the hydrogen abstraction reaction with hydrogen donor reagents. Two kinds of T_1 states that are commonly found are mainly nπ^* and $\pi\pi^*$ in nature and have been confirmed to be responsible for the observed differences in the photophysical and photochemical behavior in some BP derivatives.[3−5] The nπ^* T_1 species exhibits a high efficiency for hydrogen abstraction reaction whereas a triplet state with a $\pi\pi^*$ character typically has low reactivity for hydrogen abstraction.[6] Fenofibric acid (FA) is a hypolipidemic drug that is thought to circulate in the bloodstream after the metabolism of the commercial prodrug fenofibrate (FB).[7,8] The structures of FA and FB are shown in Scheme 1. The drug FA is a rather simple substituted BP and its ground-state absorption spectrum extends into the UV-A portion of the solar spectrum,[9] which makes FA prone to lead to photosensitized DNA damage[10] as well as peroxidation of fatty acids[11] and red blood cell hemolysis.[1] Miranda and co-workers reported that FA generally follows two different photodegradation pathways in a methanol solvent: the free acid exhibits a typical BP-like photoreactive behavior whereas its dissociated form appears to undergo a photodecarboxylation via a triplet biradical intermediate that then undergoes intramolecular electron transfer to generate a carbanion or cyclization to produce an intramolecular light-absorbing transient.[12] To help better figure out the photophysical and photochemical mechanism(s) of FA, it is useful to obtain clear assignments regarding the nature of the excited states of FA involved in the primary processes of the photochemical reactions. The aim of the present study is to characterize the photochemical pathway of the excited states of FA to gain more insight into its photochemical reactivity and behavior by directly probing the reactions using femtosecond transient absorption (fs-TA) spectroscopy and nanosecond time-resolved resonance Raman spectroscopy (ns-TR^3) on FA in acetonitrile (MeCN) and isopropyl alcohol (IPA) solvents. These results for FA are compared to previous

Received: August 8, 2011
Revised: October 28, 2011
Published: November 01, 2011

Scheme 1. Molecular Structures of FA and FB

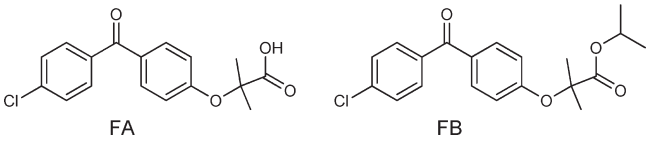

analogous results reported for BP and ketoprofen (KP) to gain more insight into structure/reactivity relationships for hydrogen abstraction reactions in a relatively inert solvent (MeCN) and a strong hydrogen donor solvent (IPA). ns-TR^3 spectra can provide useful vibrational frequency information for the fingerprint identification of the intermediates observed in the photochemical reactions of interest. Density functional theory (DFT) calculations also were carried out to better understand the properties and features of the critical intermediates.

EXPERIMENTAL AND COMPUTATIONAL METHODS

FA was obtained according to the methods reported by Scaiano and Miranda.[6] FB samples were commercially obtained from Aldrich (with 99% purity) and were used as received with spectroscopic grade MeCN and IPA to prepare various solvents for the experiments reported here. Unless noted otherwise, the sample solutions of FA and FB employed in the ns-TR^3 experiments were all with a concentration of 1.5 mM.

The fs-TA measurements were performed on the basis of a femtosecond Ti:sapphire regenerative amplified Ti:sapphire laser system (Spectra Physics, Spitfire-Pro) and an automated data acquisition system (Ultrafast Systems, Helios). The amplifier was seeded with the 120 fs output from the oscillator (Spectra Physics, Maitai). The probe pulse was obtained by using approximately 5% of the amplified 800 nm output from the Spitfire to generate a white-light continuum (350−800 nm) in a CaF_2 crystal. The intrinsic temporal resolution is 7 fs and the maximum extent of the temporal delay was 3300 ps for the optical stage used in the experiments. The instrument response function was determined to be 150 fs. At each temporal delay, data were averaged for 2 s. The probe beam is split into two before passing through the sample. One probe beam travels through the sample, the other is sent directly to the reference spectrometer that monitors the fluctuations in the probe beam intensity. Fiber optics was coupled to a multichannel spectrometer with a CMOS sensor that has a 1.5 nm intrinsic resolution. For the present experiments, the sample solution was excited by a 267 nm pump beam (the third harmonic of the fundamental 800 nm from the regenerative amplifier). The 40 mL solutions were studied in a flowing 2 mm path-length cuvette with a sample concentration of 0.32 mM throughout the data acquisition. The data were stored as three-dimensional (3D) wavelength-time-absorbance matrices that were exported for use with the fitting software.

The ns-TR^3 experiments were done using an experimental apparatus and methods discussed in detail previously,[13,14] only a brief description will be given here. The 299 nm pump laser pulse generated from the first Stokes hydrogen Raman shift laser line generated from the fourth harmonic of a Nd:YAG nanosecond pulsed laser and a 341.5 nm probe laser pulse generated from the second Stokes hydrogen Raman shift laser line from the fourth harmonic were used in the ns-TR^3 experiments. The energy for the pump and probe pulses were in the range 2.5−3.5 mJ with a 10 Hz repetition rate. The two Nd:YAG lasers were synchronized electronically by a pulse delay generator to control the time delay of the pump and probe lasers with the time delay between the laser pulses monitored by a fast photodiode and 500 MHz oscilloscope and the time resolution for the ns-TR^3 experiments was approximately 10 ns. The pump and probe laser beams were lightly focused onto the flowing sampling system and the Raman light was collected using reflective optics into a spectrometer whose grating dispersed the light onto a liquid nitrogen cooled CCD detector. The Raman signal was accumulated for 30 s by the CCD before reading out to an interfaced PC computer and 10−20 scans of the signal were added together to get a resonance Raman spectrum. The ns-TR^3 spectra presented here were obtained by the subtraction of a resonance Raman spectrum with negative time delay of −100 ns (probe-before-pump spectrum) from the resonance Raman spectrum with a positive time delay (pump−probe spectrum) and the Raman shifts were calibrated by the known MeCN solvent Raman bands with an estimated accuracy of 5 cm^{-1}. A Lorentzian function was applied to integrate the relevant Raman bands to determine the decay and growth kinetics of the species observed in the experiments.

DFT computations were used to investigate the structure and properties of the likely intermediates generated after irradiation of FA and FB in different solvents. The optimized geometries, vibrational modes, and the vibrational frequencies for the different species were obtained from (U)B3LYP DFT calculations employing a 6-311G** basis set. No imaginary frequency modes were observed at the stationary states of the optimized structures shown here. The Raman spectra were obtained using the default G03 method that used determination of Raman intensities from transition polarizabilities calculated by numerical differentiation, with assumed zero excitation frequency (e.g., using the Placzek approximation). The calculated Raman frequencies from the (U)B3LYP/6-311G** computations were scaled by a factor of 0.975 to compare with the experimental Raman results to make vibrational assignments. All of the calculations were done using the Gaussian 03 program suite.[15]

RESULTS AND DISCUSSION

Steady-State UV/Vis Spectra and fs-TA Studies on FA in MeCN. Figure 1S (Supporting Information) shows UV/vis spectra of FA recorded in neat MeCN solvent. The absorption spectrum of FA in neat MeCN has a relatively strong band with a maximum at 284 nm that is characteristic of a $\pi\pi^*$ absorbance transition and this appears significantly different from corresponding absorption spectra of KP and BP in the same solvent. FA absorbs at a higher wavelength than that of KP. A second $\pi\pi^*$ transition, found at 258 nm in MeCN solvent was also observed for FA. The difference in the relative intensities of these two $\pi\pi^*$ bands observed in the FA spectrum is very likely due to the presence of the *o*-alkyl substituent in the case of FA. It is known that the presence of an electron-donating group has little effect on the $\pi\pi^*$ band near 260 nm but induces a strong absorption at longer wavelengths.[16] In the following fs-TA experiments, the 267 nm third harmonic of the fundamental 800 nm from the regenerative amplifier was used as the pump laser.

Figure 1 displays the fs-TA spectra of FA obtained in MeCN solvent from 0 to 3000 ps delay times. To clearly indicate the spectral changes at different time scales, the dynamics of the early (within 100 ps) and late (within 3000 ps) delay times are given separately in the figure. It can be seen that the temporal evolution of the early time spectra are very similar to that of BP observed in

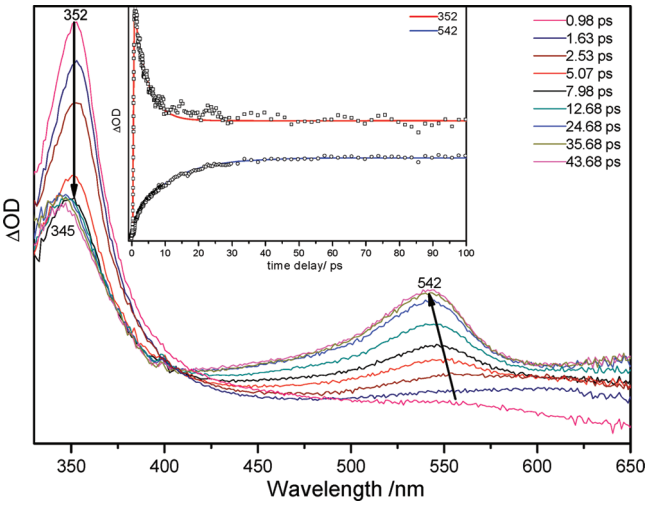

Figure 1. Transient absorption spectra of FA at early (from 0.98 to 43.68 ps) picosecond times recorded with 267 nm excitation in MeCN solvent (A). Temporal dependence of transient absorption spectra for FA recorded at early picosecond times at 352 and 542 nm are inserted at the top of the graph. The solid lines indicate the kinetics fittings to the experimental data points.

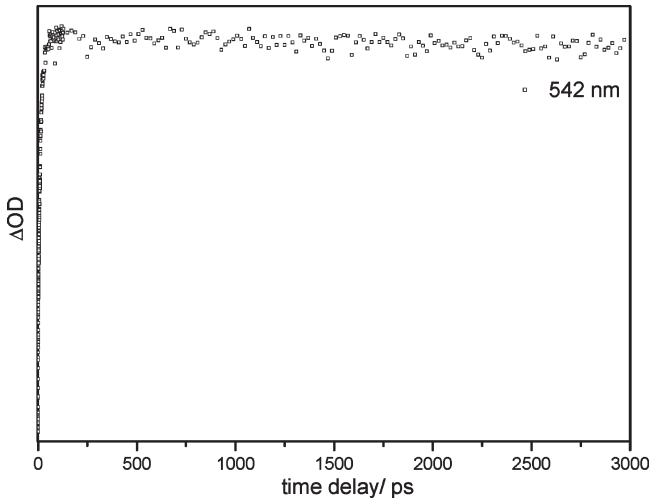

Figure 2. Temporal dependence of transient absorption spectra at 542 nm for FA recorded at later picosecond times.

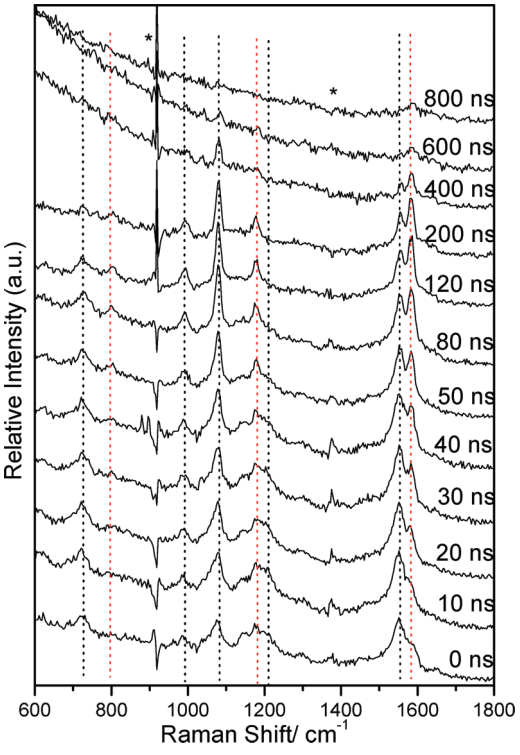

Figure 3. ns-TR^3 spectra of FA in MeCN solvent obtained with 299 nm pump excitation wavelength and 341.5 nm probe wavelength at various delay times that inserted next to the spectra. The asterisk (∗) marks subtraction artifacts and the red and black lines symbolize the different species.

MeCN solvent: one maximum absorption band (around 352 nm) grows rapidly within 1.0 ps. Later, an absorption band (around 542 nm) grows within 60 ps at the expense of the band around 352 nm. With the degradation of the 352 nm transient absorption, this peak gradually shifts to 345 nm. After the beginning of 60 ps, the two transient absorptions at 345 and 542 nm begin to be stable until 3000 ps; these two transient absorptions are contributed from the triplet state FA (^{3}FA). The growth kinetics of the transient absorption at 352 nm can be fit by one exponential function with a ca. 0.28 ps time constant in MeCN solvent. The spectrum at very early time (such as 0.98 ps spectrum in Figure 1) is assigned to the $S_1 \rightarrow S_n$ transition absorption from the S_1 ($n\pi^*$) singlet state. With the reduction of the S_1 signal, the subsequent changes in the spectra are mainly attributed to the $S_1 \rightarrow T_1$ ISC process that leads to the increase of the transient absorption at 542 nm, which is similar to the well-known BP's transient absorption that corresponds to the $T_1 \rightarrow T_n$ transition with a maximum at 330 and 525 nm in neat MeCN solvent.[17] The dynamics of the formation for the T_1 states is monitored at 542 nm, and the result is inserted in Figure 1 together with its exponential fittings of the experimental data points. The fully developed spectra for the absorption at 542 nm can be fitted by a two exponential function with time constants of $t_1 = 0.28$ ps, $t_2 = 11$ ps in neat MeCN solvent. The short growth time (ca. 0.28 ps) is due to the ultrafast internal conversion (IC) from S_n directly to S_1 (S_1 also has contribution at the 542 nm wavelength), and the longer one (ca. 11 ps) is attributed to the ISC from the S_1 to T_1 transition. The ISC time constant (ca. 11 ps) in MeCN solvent from S_1 to T_1 transition is very close (within experimental uncertainty in the measurement) to the ISC time constant (10 ps) observed for BP,[18] and this implies that the substituents in the aromatic ring of FA have little influence on the rate of ISC comparison to that of BP. The triplet assignment is also confirmed by the behavior in the later decay time in MeCN solvent. After the generation of ^{3}FA, the fs-TA spectra recorded in MeCN solvent show very little change at late picosecond times up to 3000 ps (Figure 2), which is consistent with previously reported results that the ^{3}FA species was still observed by nanosecond laser flash photolysis (LFP) absorption spectra.[16] This verifies that the triplet is the reactive precursor species to the photochemistry events in the nanosecond times.[19]

ns-TR^3 Spectra of FA in Nonaqueous Solutions. *A. ns-TR^3 Spectra of FA in the MeCN Solvent.* FA consists of a substituted BP in its structure and is thought to have a BP-like photochemical

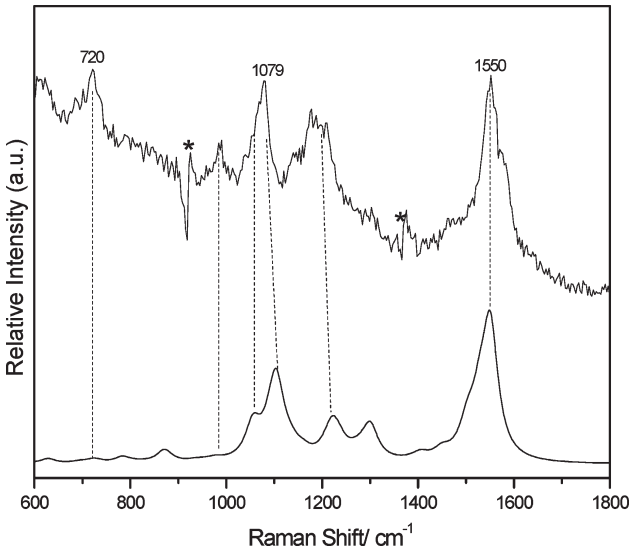

Figure 4. Comparison the experimental resonance Raman spectrum of FA (top) obtained in the MeCN solvent at 10 ns delay time with the DFT calculated spectrum for the triplet species. Dotted lines display the correlation between the experimental and calculated Raman bands. The asterisk (∗) marks subtraction artifacts.

behavior in MeCN solvent (a relatively inert solvent). The $n\pi^*$ triplet state of BP and KP (^{3}BP and ^{3}KP) are observed in relatively inert solvent like MeCN and then decay by either photophysical pathways or by oxygen quenching.[18,20−22] Figure 3 shows an overview of the ns-TR^3 spectra for the excitation of 1.5 mM FA in MeCN. Two species are observed from 0 to 800 ns. The first species appears nearly at 0 ns and has its strongest bands at 720, 1079, and 1550 cm^{-1} and a broad band in proximity to 1200 cm^{-1}. According to the results of the fs-TA spectra at late picosecond times, this species can be assigned to the ^{3}FA species. Comparison of the experimental resonance Raman spectra of FA obtained in the MeCN solvent at 10 ns and the DFT calculated spectrum for the ^{3}FA species (shown in Figure 4) shows a good agreement for their vibrational frequency pattern, and this implies that the first species assignment to the ^{3}FA intermediate is reasonable. As for the ^{3}FA intermediate, most of the Raman bands observed in the ns-TR^3 spectra are due to vibrations associated with the C−C stretch; C−O stretch; C−Cl stretch vibrational modes and C−H bend motions. The UB3LYP/6-311G** calculation predicts that the 1550 cm^{-1} Raman band is mainly due to the ring C−C stretching vibrational mode. The broad Raman band close to 1200 cm^{-1} is mostly due to a triplet carbonyl C−O stretch vibrational mode. The 1079 cm^{-1} Raman band is due to the C−H bend and C−Cl stretching vibrational motions in the substituted aromatic ring. The 720 cm^{-1} Raman band is due to the ring breathe stretching bend of aromatic ring. The second species having its strong Raman bands at 728, 758, 806, 995, 1082, 1121, 1177, 1558, and 1583 cm^{-1} is more likely a ketyl radical species. The identification of this species will be discussed in the following section.

B. Comparison Reactivity for the Triplet State of BP, KP, and FA. ^{3}BP, ^{3}KP, and ^{3}FA were observed in the MeCN solvent by the ns-TR^3 experiments. They are excited from a $\pi\pi^*$ transition to the $n\pi^*$ S_1 which subsequently undergo fast ISC to form T_2 with a $\pi\pi^*$ character. The IC process then takes place to form the $n\pi^*$ nature T_1 triplet state with hydrogen abstraction ability.[20,23−25]

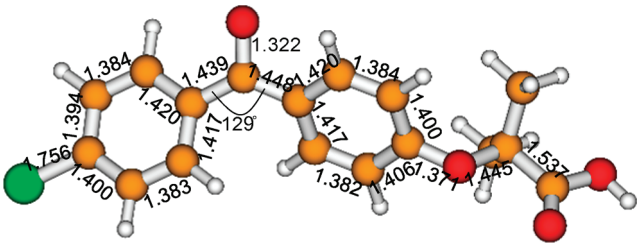

Figure 5. Optimized structure of ^{3}FA obtained from the UB3LPY/6-311G** calculations. Selected bond lengths and angles display in the structure.

The ns-TR^3 experiments were performed in the MeCN solvent where the hydrogen abstraction reaction to produce the diphenyl ketyl radical did not occur and ^{3}BP only seemed to decay substantially by either a photophysical pathways or a quenching reaction by oxygen dissolved in the MeCN solvent .[20] However, besides the observation of ^{3}KP, a very weak species was observed from 20 ns with the decay of ^{3}KP. Both ^{3}BP and ^{3}KP can last for around 300 ns in the MeCN solvent under ambient conditions. Unlike the dynamics of ^{3}BP and ^{3}KP, the ^{3}FA species decays very fast and disappears within about 120 ns. The decay of ^{3}FA results in a new species that begins to arise at 20 ns. This reveals that the ^{3}FA intermediate is the precursor of the second species observed in the MeCN solvent. No observation of a ketyl radical intermediate indicates that the ^{3}BP species does not easily abstract hydrogen from the MeCN solvent. The ^{3}KP species appears to have weak hydrogen abstraction ability in the MeCN solvent with a minor species being observed after the decay of ^{3}KP, and this minor species probably results from either intermolecular or intramolecular hydrogen abstraction among KP molecules. High and low concentration (4 and 2 mM) ns-TR^3 experiments demonstrate that intermolecular hydrogen abstraction is not likely to occur, and the weak species might arise from an intramolecular hydrogen abstraction on the side chain in KP.[21] As for the ^{3}FA intermediate, the side chain is on the para position in the benzene ring so the intramolecular hydrogen abstraction is difficult due to the long distance between the carbonyl group and the side chain. The concentration of FA (1.5 mM) is even lower than that of KP in the ns-TR^3 experiments reported previously, whereas the clear observation of second species after the decay of the ^{3}FA intermediate indicates that ^{3}FA shows a relative higher hydrogen abstraction ability than ^{3}BP and ^{3}KP in the MeCN solvent. A possible reason is that the substituents on the benzene ring strongly affect the reactivity of ^{3}FA. Here, Cl is an electron withdrawing group located at the para position in the benzene ring and it has been reported previously that electron-withdrawing groups generally increase the photoreduction ability of the substituted ^{3}BP.[26,27] For example, the decafluoro-BP derivative was found to be 10−40 times more reactive than the parent BP molecule,[26,27] On the other hand, the −OR group located at the para position in another benzene ring is an electron donor group. Electron donating groups with lone pairs on the atoms adjacent to the π system activate the aromatic ring by increasing the electron density on the ring through a resonance donating effect. The resonance only allows electron density to be positioned at the ortho and para positions. After the formation of the ketyl radical at C_7 (labels for the number of the atoms of FA are shown in Figure 2S in the Supporting Information) of the carbonyl group, the radical could be stabilized by the presence of

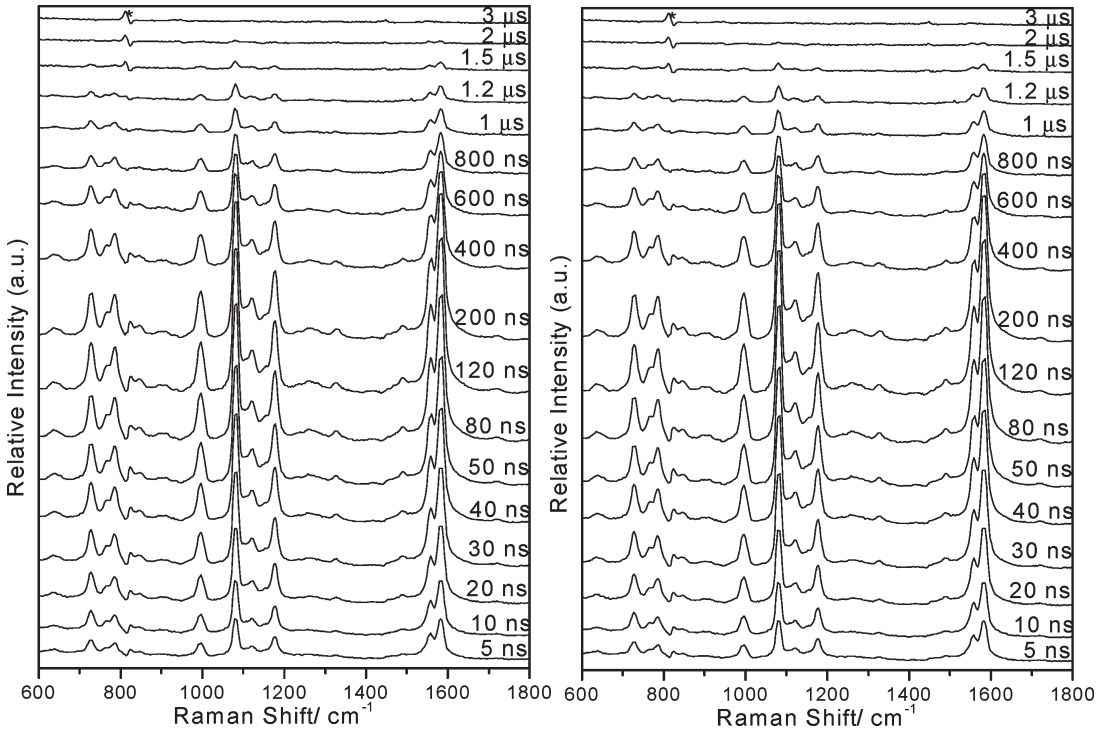

Figure 6. ns-TR^3 of FA (left) and FB (right) in IPA obtained with 299 nm pump excitation wavelength and 341.5 nm probe wavelength at various delay times that indicated next to the spectra. The asterisk (∗) marks subtraction artifacts.

the relatively higher electron density at the para position (C_9) relative to C_{12}−OR. By the cooperation of these two effects, the resonance Raman signal for the second species of FA is significant stronger than that of BP and KP.

Figure 5 shows the UB3LPY/6-311G** calculated optimized structure of ^{3}FA, the substituents on the parent of BP in the ^{3}FA species result in significant perturbations on the overall Raman spectra and structure compared to those of BP and KP. The C−C bonds length of the benzene ring with the chlorine atom are obviously longer than those of ^{3}BP and ^{3}KP, whereas the benzene ring with the *o*-alkyl substituent exhibits more quinonoidal character than those of ^{3}BP and ^{3}KP (comparisons of the bond lengths are shown in Table 1S, Supporting Information).[21] The C═O bond length in the carbonyl group is 1.322 Å, which is obviously shorter than the ones of ^{3}BP and ^{3}KP (1.330 Å for ^{3}BP and 1.329 Å for ^{3}KP). This may be the reason the ^{3}FA species exhibits a significantly stronger hydrogen abstraction activity toward the ground state FA or MeCN solvent compared to the ^{3}BP and ^{3}KP intermediates. Previous studies reported that the frequency of the C═O stretch mode appears in the 1400−1600 cm^{-1} range for a $\pi\pi^*$ dominated triplet states and in the 1200−1400 cm^{-1} region for typical nπ^* nature triplet states.[28−31] As illustrated above, the C═O stretching frequency predicted and observed for the carbonyl group for the ^{3}FA intermediate is close to 1200 cm^{-1}, and this demonstrates that the ^{3}FA species has a typical nπ^* dominated configuration in the MeCN solvent and this is consistent with a nπ^* ^{3}FA species observed in the MeCN solvent at subnanosecond times by the fs-TA spectra. For aromatic carbonyl compounds, the electronic configuration of the T_1 state determines the T_1 state's reactivity toward the hydrogen abstraction reaction with hydrogen donor reagents. Two types of T_1 states, dominated respectively by nπ^* and $\pi\pi^*$ character, have been identified to be responsible for the differences in the photophysical and photochemical behavior of these triplets. The known chemistry of the ^{3}BP derivative acids, including decarboxylation and hydrogen abstraction, occurs predominantly from the nπ^* triplet state whereas a triplet state with a $\pi\pi^*$ nature is barely reactive for those types of reaction.[6] As a consequence, a typical nπ^* character causes ^{3}FA to have a higher activity and even in the MeCN solvent, ^{3}FA can abstract a hydrogen from the ground state FA or MeCN solvent.

C. ns-TR^3 of FA and FB in the Stronger Hydrogen Donor Solvent: Generation of Ketyl Radical from the Intermolecular Hydrogen Abstraction. IPA is a strong hydrogen donor solvent, the results of the ns-TR^3 experiments indicate that intermolecular hydrogen abstraction would take place as for ^{3}BP and ^{3}KP in the IPA solvent and produce a ketyl radical intermediate.[20,21] Figure 6 shows the ns-TR^3 spectra of 1.5 mM FA acquired by the irradiation of FA in neat IPA. Only one intermediate is observed from 5 to 3000 ns. This species associated with its most intense bands at 728, 758, 995, 1082, 1121, 1177, 1558, and 1583 cm^{-1} is thought to be the FA ketyl radical. Figure 7 displays a comparison of Raman spectra of FA obtained at delay time of 200 ns and the calculation predicted Raman spectra of the FA ketyl radical. Inspection of Figure 7 clearly shows that the experimental resonance Raman spectra of FA in IPA are very similar with that of the calculation predicted Raman spectra of the FA ketyl radical only with some moderate frequency shifts. The satisfactory agreement of the experimental and calculated Raman spectra demonstrates that the intermediate of FA observed in IPA can be assigned to the FA ketyl radical. The key optimized structural parameters of the FA ketyl radical with selected bond lengths and angles are shown in Figure 8. The second intermediate observed in the MeCN solvent has the same resonance Raman bands with the one obtained in the IPA solvent; therefore, this implies that the ^{3}FA intermediate should experience the hydrogen

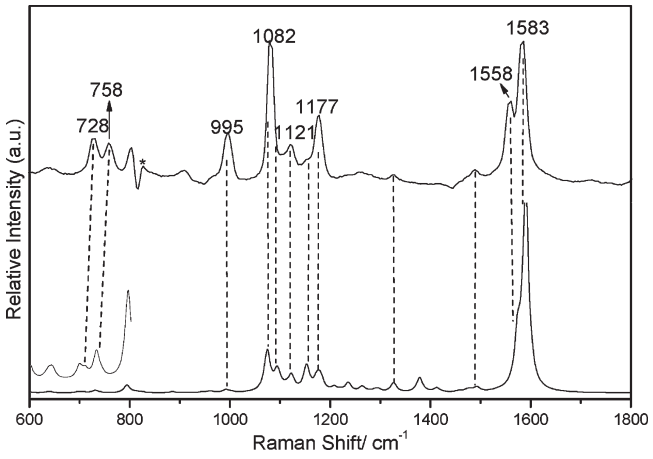

Figure 7. Comparison resonance Raman spectra of FA (top) obtained in IPA at 200 ns with the calculation predicted Raman spectra of the ketyl radical of FA (bottom). Inserted at bottom of left is the magnification of the lower frequency. The asterisk (∗) marks subtraction artifacts.

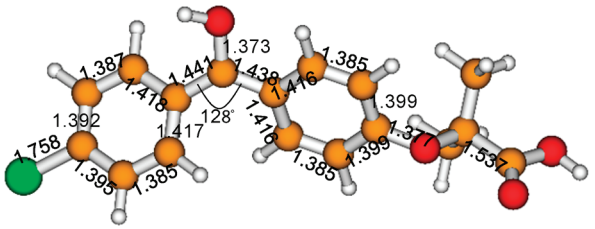

Figure 8. Optimized structure of the FA ketyl radical calculated by UB3LPY/6-311G**. Selected bond lengths and angle display in the structure.

abstraction reaction with the ground state FA or the MeCN solvent to generate a FA ketyl radical. Most of the Raman bands seen in the TR^3 spectra of the FA ketyl radical intermediate are due to the vibrations associated with the ring C−C stretch, C−O stretch, C−Cl stretch, and C−H bend motions. The 1558 and 1583 cm^{-1} Raman bands are mainly due to a ring C−C stretch vibrational mode. The 1326 cm^{-1} Raman band is mostly contributed from a C−O (the OH group between two benzenes) stretching mode. The 1177 and 1121 cm^{-1} Raman bands are associated with a C−H in-plane bending of the ring vibration motion. The stronger Raman band at 1082 cm^{-1} is associated with a C−Cl stretch vibrational mode. The 995 cm^{-1} Raman feature is attributed to the C−C ring deformation mode of the benzene ring with chlorine substituent. The 728 and 758 cm^{-1} Raman bands belong to the ring breath vibrational mode.

Examination of the ns-TR^3 spectra implies that the intermolecular hydrogen abstraction exhibits a much higher efficiency in the stronger hydrogen donor solvent (IPA) compared with the more inert MeCN solvent, and this accounts for the faster appearance and stronger resonance Raman signal of the FA ketyl radical in the IPA solvent than in the MeCN solvent. The observation of the FA ketyl radical gives direct support to the fact that the ^{3}FA species has a particularly dominant nπ^* nature and decays very fast in the IPA solvent, this correlates with a fast growth time constant (ca. 60 ns) for the FA ketyl radical. The FA ketyl radical species has a ca. 450 ns decay time constant

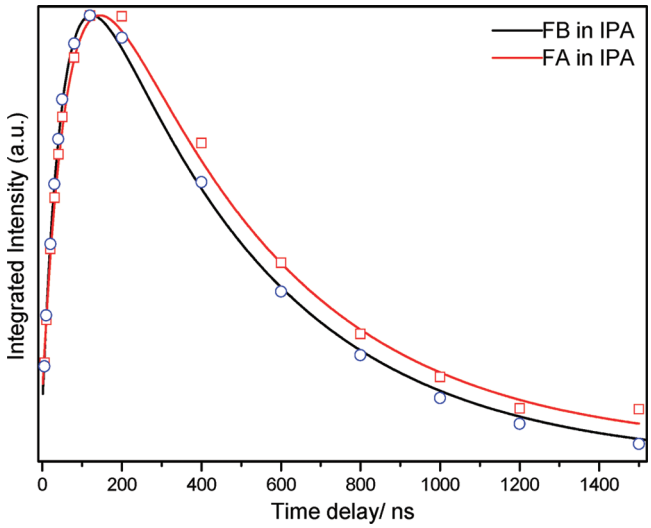

Figure 9. Time dependence of the resonance Raman band at 1583 cm^{-1} for FA (closed squares) and FB (closed circle) in IPA fit by a two-exponential function with a ca. 68 ns growth time constant and ca. 450 ns decay time constant for FA and a ca. 53 ns growth time constant and ca. 446 ns decay time constant for FB. The solid lines indicate the kinetics fitting to the experimental data points.

and completely disappears at about 2 μs (Figure 9). The light absorption transient (LAT) is not readily observed in the IPA solution, probably due to the two para positions of the benzene ring being occupied, whereas a LAT species could last for a long lifetime after the photolysis of BP and KP in IPA solvent.[20,21]

To further confirm the occurrence of the hydrogen abstraction reaction, ns-TR^3 experiments were also carried out for FB in IPA. FB is the ester of FA and exhibits very similar TR^3 spectra (Figure 6) in comparison to that of FA except for a blue shift 786 cm^{-1} Raman band that is mainly associated with the ring breathing vibrational motion of the benzene ring with the *o*-alkyl substituent and the C−O bend vibrational mode from the ester. FB is a good control compound because it does not undergo the decarboxylation and rearrangement that may take place following the photolysis of the FA anion.[6,32] Only the hydrogen abstraction pathway can proceed for FB in the IPA solvent and a ketyl radical species of FB is observed, and this intermediate has ca. 53 ns for the growth time constant and ca. 446 ns for the decay time constant, which are close to those of FA in IPA. The control experiment provides important evidence to support the generation of the FA ketyl radical by an intermolecular hydrogen abstraction reaction for FA. The FA and FB ketyl radicals have growth time constants of ca. 60 ns and ca. 53 ns, respectively, under the experimental conditions employed here. The relatively short growth time implies that the ^{3}FA and ^{3}FB intermediates can be readily photoreduced by the hydrogen-donor IPA solvent to form the ketyl radical species.

CONCLUSION

The photochemistry of FA in the MeCN and IPA solvents was explored using the fs-TA and ns-TR^3 spectroscopy. A strong transient absorption at 352 nm, which is associated with $S_1 \rightarrow S_n$ is observed in the MeCN solvent and then it undergoes intersystem crossing (11 ps time constant) to transform into two transient absorption peaks at 345 and 542 nm that are contributed

to $T_1 \rightarrow T_n$. Thus a $n\pi^*$ ^{3}FA intermediate is evolved in the late picosecond times and early nanosecond times, which is observed and confirmed by the ns-TR^3 experiment. The $n\pi^*$ ^{3}FA displays a higher reactivity than ^{3}BP and ^{3}KP in the MeCN solvent. Hydrogen abstraction will occur for the $n\pi^*$ ^{3}FA and a FA ketyl radical will be generated in the MeCN solvent. However, the $n\pi^*$ ^{3}FA is hardly observed in the resolution of the ns-TR^3 instrument in IPA solvent, which promptly abstracts a hydrogen from IPA solvent to generate a ketyl radical intermediate. Because two para positions are occupied, the LAT intermediate has not yet observed in the IPA solvent with the decay of the FA ketyl radical.

■ ASSOCIATED CONTENT

Supporting Information. Figure 1S: UV/vis spectra of FA in the MeCN and IPA solvent with labels on the top right corner. Figure 2S: Labels for the number of the atom of FA. Figure 3S: The Cartesian coordinate, total energies, and vibrational zero-point energies for the optimized geometry from the (U)B3LYP/6-311G** calculations for the species of interest in the paper are given. Table 1S: Selected bond length (Å) parameters for some species observed in the photochemistry of FA, KP, and BP. This material is available free of charge via the Internet at http://pubs.acs.org.

■ AUTHOR INFORMATION

Corresponding Author
*Telephone: 852-2859-2160. Fax: 852-2857-1586. E-mail: phillips@hku.hk.

■ ACKNOWLEDGMENT

This work was supported by a grant from the Research Grants Council of Hong Kong (HKU 7035/08P) and the University Grants Committee Special Equipment Grant (SEG-HKU-07) to D.L.P. Support from the University Grants Committee Areas of Excellence Scheme (AoE/P-03/08) is also gratefully acknowledged.

■ REFERENCES

(1) Bosca, F.; Miranda, M. A. *J. Photochem. Photobiol. B. Biol.* **1998**, *43*, 1–26.
(2) Cosa, G. *Pure Appl. Chem.* **2004**, *76*, 263–275.
(3) Wagner, P. J.; Puchalski, A. E. *J. Am. Chem. Soc.* **1980**, *102*, 6177–6178.
(4) Wagner, P. J.; Siebert, E. J. *J. Am. Chem. Soc.* **1981**, *103*, 7329–7335.
(5) Wagner, P. J.; Truman, R. J.; Puchalski, A. E.; Wake, R. *J. Am. Chem. Soc.* **1986**, *108*, 7727–7738.
(6) Cosa, G.; Purohit, S.; Scaiano, J. C.; Bosca, F.; Miranda, M. A. *Photochem. Photobiol.* **2002**, *75*, 193–200.
(7) Kloer, H. U. *Am. J. Med.* **1987**, *83*, 3–8.
(8) Elsom, L. F.; Hawkins, D. R.; Chasseaud, L. F. *J. Chromatogr.* **1976**, *123*, 463–467.
(9) Porter, G. In *Light, Chemical Change and Life: a Source Book in Photochemistry*; Coyle, J. D., Hill, R. R., Roberts, D. R., Eds.; The Open University Press: Milton Keynes, U.K., 1982.
(10) Maguery, M. C.; Chouini-Lalanne, N.; Ader, J. C.; Paillous, N. *Photochem. Photobiol.* **1998**, *68*, 679–684.
(11) Miranda, M. A.; Bosca, F.; Vargas, F.; Canudas, N. *Photochem. Photobiol.* **1994**, *59*, 171–174.
(12) Bosca, F.; Miranda, M. A. *Photochem. Photobiol.* **1999**, *70*, 853–857.
(13) Chan, P. Y.; Ong, S. Y.; Zhu, P.; Zhao, C. Y.; Phillips, D. L. *J. Phys. Chem. A* **2003**, *107*, 8067–8074.
(14) Zhu, P. Z.; Ong, S. Y.; Chan, P. Y.; Leung, K. H.; Phillips, D. L. *J. Am. Chem. Soc.* **2001**, *123*, 2645–2649.
(15) Frisch, M. J.; Trucks, G. W.; Schlegel, H. B.; Scuseria, G. E.; Robb, M. A.; Cheeseman, J. R.; Montgomery, J. A., Jr.; Vreven, T.; Kudin, K. N.; Burant, J. C.; Millam, J. M.; Iyengar, S. S.; Tomasi, J.; Barone, V.; Mennucci, B.; Cossi, M.; Scalmani, G.; Rega, N.; Petersson, G. A.; Nakatsuji, H.; Hada, M.; Ehara, M.; Toyota, K.; Fukuda, R.; Hasegawa, J.; Ishida, M.; Nakajima, T.; Honda, Y.; Kitao, O.; Nakai, H.; Klene, M.; Li, X.; Knox, J. E.; Hratchian, H. P.; Cross, J. B.; Bakken, V.; Adamo, C.; Jaramillo, J.; Gomperts, R.; Stratmann, R. E.; Yazyev, O.; Austin, A. J.; Cammi, R.; Pomelli, C.; Ochterski, J. W.; Ayala, P. Y.; Morokuma, K.; Voth, G. A.; Salvador, P.; Dannenberg, J. J.; Zakrzewski, V. G.; Dapprich, S.; Daniels, A. D.; Strain, M. C.; Farkas, O.; Malick, D. K.; Rabuck, A. D.; Raghavachari, K.; Foresman, J. B.; Ortiz, J. V.; Cui, Q.; Baboul, A. G.; Clifford, S.; Cioslowski, J.; Stefanov, B. B.; Liu, G.; Liashenko, A.; Piskorz, P.; Komaromi, I.; Martin, R. L.; Fox, D. J.; Keith, T.; Al-Laham, M. A.; Peng, C. Y.; Nanayakkara, A.; Challacombe, M.; Gill, P. M. W.; Johnson, B.; Chen, W.; Wong, M. W.; Gonzalez, C.; Pople, J. A. *Gaussian 03*, revision D.01; Gaussian, Inc.: Wallingford, CT, 2004.
(16) Lhiaubet, V.; Gutierrez, F.; Berruyer, P. F.; Amouyal, E.; Daudey, J. P.; Poteau, R.; Chouini-Lalanne, N.; Paillous, N. *New J. Chem.* **2000**, *24*, 403–410.
(17) Aloise, S.; Ruckebusch, C.; Blanchet, L.; Rehault, J.; Buntinx, G.; Huvenne, J. P. *J. Phys. Chem. A* **2008**, *112*, 224–231.
(18) Shah, B. K.; Rodgers, M. A. J.; Neckers, D. C. *J. Phys. Chem. A* **2004**, *108*, 6087–6089.
(19) Ma, C.; Kwok, W. M.; Chan, W. S.; Du, Y.; Kan, W. J. T.; Toy, P. H.; Phillip, D. L. *J. Am. Chem. Soc.* **2006**, *128*, 2558–2570.
(20) Du, Y.; Ma, C.; Kwok, W. M.; Xue, J.; Phillips, D. L. *J. Org. Chem.* **2007**, *72*, 7148–7156.
(21) Chuang, Y. P.; Xue, J.; Du, Y.; Li, M. D.; An, H. Y.; Phillips, D. L. *J. Phys. Chem. B* **2009**, *113*, 10530–10539.
(22) Wolfbeis, O. S.; Furlinger, E. *J. Am. Chem. Soc.* **1982**, *104*, 4069–4072.
(23) Shah, B. K.; Neckers, D. C. *J. Am. Chem. Soc.* **2004**, *126*, 1830–1835.
(24) Okustu, T.; Muramatsu, H.; Horiuchi, H.; Hiratsuka, H. *Chem. Phys. Lett.* **2005**, *404*, 300–303.
(25) Cai, X.; Sakamoto, M.; Hara, M.; Sugimoto, A.; Tojo, S.; Kawai, K.; Endo, M.; Fujitsuka, M.; Majita, T. *Photochem. Photobiol. Sci.* **2003**, *2*, 1209–1214.
(26) Shoute, L. C. T.; Mittal, J. P. *J. Phys. Chem.* **1993**, *97*, 8630–8637.
(27) Anandhi, R; Umapathy, S *J. Raman Spectrosc.* **2000**, *31*, 331–338.
(28) Webb, S. P.; Yeh, S. W.; Phillips, L. A.; Tolbert, M. A.; Clark, J. H. *J. Am. Chem. Soc.* **1984**, *106*, 7286–7288.
(29) Webb, S. P.; Phillips, L. A.; Yeh, S. W.; Tolbert, L. M.; Clark, J. H. *J. Phys. Chem.* **1986**, *90*, 5154–5164.
(30) Schwartz, B. J.; Peteanu, L. A.; Harris, C. B. *J. Phys. Chem.* **1992**, *96*, 3591–3598.
(31) Toscano, J. P. In *Reviews of Reactive Inermediate Chemistry*; Platz, M. S., Moss, R. A., Jones, M., Jr., Eds.; John Wiley and Sons, Inc.: Hoboken, NJ, 2007.
(32) Vargas, F.; Canudas, N.; Miranda, M. A.; Bosca, F. *Photochem. Photobiol.* **1993**, *58*, 471–476.